Parameter-dependent multichannel Rydberg spectra

Qiaoling Wang
Joint Institute for Laboratory Astrophysics, University of Colorado, Boulder, Colorado 80309
and Department of Physics and Astronomy, Louisiana State University, Baton Rouge, Louisiana 70803

Chris H. Greene
Department of Physics and Joint Institute for Laboratory Astrophysics, University of Colorado, Boulder, Colorado 80309
(Received 13 March 1991)

A variety of complex spectral features occurs in multichannel Rydberg systems when the ionization thresholds vary in a simple manner with a tunable parameter such as the magnetic-field strength. We develop an analytical description of these features, identifying the key dynamical quantities controlling the appearance of "complex resonances" and their evolution with the parameter. The analysis predicts a ubiquitous occurrence of states with vanishing autoionization width, and of multiple q reversals associated with perturbing configurations. This description can be used to interpret some features of the diamagnetic spectrum of lithium near the zero-field ionization threshold.

I. INTRODUCTION

A recent experiment on the strikingly complex near-threshold photoabsorption spectrum of lithium in a strong magnetic field [1] provides a new handle which helps greatly to unravel its complexity. The unexpectedly regular pattern of the spectrum traced simultaneously versus energy and versus the magnetic-field strength indicates that its complexity results from strong interactions among Rydberg states converging to different Landau thresholds. Specifically, the strong interaction between these levels in many Landau channels shows constructive and destructive interference between multiple autoionization pathways. This phenomenon is very common in atomic and molecular systems [2–8], where it has been called a "complex resonance," or "overlapping resonance." The Landau energy levels of a free electron in the magnetic field have the form $E_n^{(L)}=(\omega_c/2)(2n+m+|m|+1)$ a.u., where ω_c is the cyclotron frequency ($\omega_c=B/B_0$ with $B_0=2.35\times10^5$ T) and where m is the magnetic quantum number. As shown in Refs. [9] and [10], these Landau levels act as ionization threshold energies, with an infinity of Rydberg levels converging to each one.

For the specific problem of Rydberg state diamagnetism at $B\approx6$ T, a very recent calculation of Delande *et al.* [11,12] has achieved for the first time impressive agreement with experimental observations [1] above the ionization threshold to spectroscopic accuracy. This large-scale diagonalization, like those performed previously to describe the photoabsorption spectrum below threshold [13], gives added confidence in the measured spectrum, but it has not yet succeeded in giving a qualitative interpretation of the diverse, complicated spectral features. Most of the interpretive progress has come instead from the calculations [14–17] that determined the most important periodic orbits from the viewpoint of classical mechanics augmented by the Gutzwiller formula [17]. These treatments explain the major peaks occurring in the Fourier transform of the photoabsorption spectrum plotted versus the energy, particularly those features limited to short periods $T\lesssim10T_c$, where T_c is the cyclotron period. The very-high-resolution spectrum of Li obtained by Refs. [1] and [18] shows numerous narrow resonances and other regularities occurring at far greater time scales not amenable to this classical viewpoint.

The present paper shows how a spectrum of the type observed by Ref. [1] can be described as a conventional, multichannel, perturbed Rydberg spectrum. We show how a number of complex and interesting features can arise, quite generally, when the ionization thresholds vary with a parameter such as the magnetic-field strength. These features include changes in the intensity, width, and shape of each individual resonance within a complex resonance, when traced along the magnetic field. Multichannel Rydberg spectra with parameter-dependent thresholds have hardly been treated to date, but they encompass phenomena beyond the field dependences considered in this paper, such as the variation of the electronic terms of a diatomic molecule as a function of the internuclear distance [19].

Before Sec. III discusses atomic photoabsorption in a strong magnetic field, Sec. II first presents a detailed multichannel quantum-defect theory (MQDT) description of three interacting channels, one of which is open while the other two are closed. Many readers may not be interested in the details of Sec. II, and can proceed to Sec. III. But we have found it necessary to modify the definition of shape and width parameters of individual resonances, which had been previously identified by Giusti-Suzor and co-workers [20,21]. As in Refs. [20] and [21], the analysis in Sec. II starts from a smooth, short-range reaction matrix K, of the type familiar in MQDT formulations, which is assumed to be independent of energy and mag-

netic field. The K matrix is normally obtained from an *ab initio* calculation [22–24], but since this is not the main goal of this paper, we suppose that it has been obtained elsewhere. A Beutler-Fano profile $\sigma=\sigma_0(\varepsilon+q)^2/(1+\varepsilon^2)$ is used to parametrize each individual resonance within a complex perturber. The line-shape parameter q, and the width parameter Γ included in the definition of $\varepsilon\equiv(E-E_R)/\frac{1}{2}\Gamma$, can be expressed analytically in terms of quantities that remain relatively smooth across a complex resonance.

In Sec. III, we consider the evolution of a complex resonance whose ionization thresholds are proportional to the magnetic-field strength. Many interesting features in the calculated model three-channel spectrum, namely intensity, width, and line-shape variations with energy and field, can be characterized in terms of the parameters introduced in Sec. II. Some of these features can be found in the experimental spectrum [1] as well. Clearly, the restriction to three channels, and the assumption of a reaction matrix K independent of E and B, are both oversimplifications. In fact, atomic hydrogen (or lithium) at $B=6$ T probably involves more like 20–30 channels. Yet this three-channel model provides the simplest prototype system which gives the main features of complex autoionizing resonances, and which illustrates the effect of parameter-dependent thresholds. Moreover, since we consider only a very narrow range of B and E, it is reasonable to approximate the K matrix by a constant matrix. Section III also includes a model calculation with twenty interacting channels for field strengths near $B=6$ T, which shows that such a model does indeed generate spectra bearing a qualitative resemblance to those seen experimentally in Ref. [1].

II. PROPERTIES OF PERTURBED RYDBERG SERIES: A THREE-CHANNEL MODEL ANALYSIS

In this section, we develop a set of parameters to describe a perturbed autoionizing Rydberg series of a three-channel system. For alternative discussions of many-channel system from a different (level-by-level) point of view, see Fano [25], Fano and Cooper [26], Mies [27], and Connerade [28]. These parameters include a line-shape parameter q for each individual resonance, and a smooth reduced-width function $\Gamma_s^{(r)}$. The q parameter is found to be very energy dependent, as, in particular, it can change sign (the so-called q reversals) in two ways. One is the smooth change at a zero of q; the other is the rapid change at a pole of q. The two different types of q reversals cause different features in the spectrum. The smooth reduced-width function itself displays an asymmetric shape reminiscent of a Beutler-Fano profile. This asymmetry manifests the interference effects of different autoionizing pathways when the Rydberg series is perturbed by an interloper. The energies of "zero-width" resonances can be predicted by this function.

Figure 1 shows the zeroth-order picture of Rydberg series converging to three nondegenerate ionization thresholds $E_1<E_2<E_3$. We are primarily interested in the energy range where the total energy E is slightly below the second ionization threshold E_2. The key

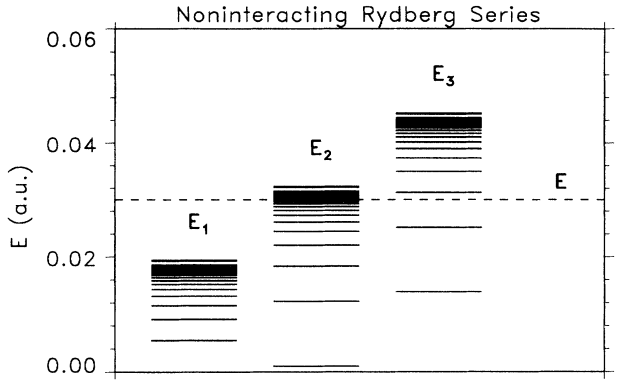

FIG. 1. Zeroth-order picture of a Rydberg series converging to three ionization thresholds $E_1<E_2<E_3$.

features in this energy range are governed by the fact that the spectral variations associated with Rydberg structures in channel 2 occur on a very small characteristic energy scale $\Delta\varepsilon_2\sim\nu_2^{-3}$. Here the effective quantum number in channel i is defined by

$$\nu_i=[-2(E-E_i)]^{-1/2}\ , \tag{1}$$

where the energies are in a.u. On the other hand, the characteristic scale for spectral variations associated with channel 3 is much larger, namely $\Delta\varepsilon_3\sim\nu_3^{-3}$. It is this interplay between two greatly differing energy scales (and correspondingly different time scales, $\Delta t\sim\nu_i^3$, and different distance scales, $\Delta r\sim\nu_i^2$) that is responsible for the striking appearance and much of the qualitative physics associated with such spectra [2–8].

In this energy range near the second ionization threshold E_2, the states associated with the third channel play a role as "perturbers," or "interlopers," into the Rydberg series of the second channel, which we denote the "host" Rydberg series using the terminology of Giusti-Suzor and Lefebvre-Brion [21]. In our analysis, we isolate the effects of states in the third channel as causing a characteristic energy dependence of the "individual" level intensities, line shapes, and reduced autoionization widths of the host Rydberg series. This viewpoint is appropriate here, since in the absence of the perturbers, these would all be constants (provided the K matrix is constant) [20]. To state it more clearly, we initially "eliminate" the third channel in the usual sense of the MQDT, which means specifically that a linear combination of the K-matrix states is found such that the closed-channel components of the wave function in the third channel decay exponentially at $r\rightarrow\infty$. After the third channel is eliminated, its effects are fully incorporated as energy dependences in the remaining two-channel reaction matrix. The remainder of the analysis can then proceed along the lines of previous two-channel analyses [20]. This two-step procedure differs from previous studies of three-channel systems by Giusti-Suzor and Lefebvre-Brion [21], by Cooke and Cromer [29], and by Wintgen and Friedrich [30], all of whom treat the two closed channels on an equal foot-

ing. Since the order of applying asymptotic boundary conditions in the closed channels is irrelevant, eliminating these closed channels one by one is equivalent to eliminating all of them simultaneously. However, eliminating the two channels separately helps to keep track of the two qualitatively different energy scales in the problem, as will be seen below. After eliminating the third channel, the energy-dependent 2×2 reaction matrix and dipole matrix, denoted as $\tilde{K}$ and $\tilde{d}$, are given according to Seaton's formula [31]:

$$\tilde{K}=\begin{bmatrix} K_{11}-\dfrac{K_{13}K_{31}}{T_3} & K_{12}-\dfrac{K_{13}K_{32}}{T_3} \\ K_{21}-\dfrac{K_{23}K_{31}}{T_3} & K_{22}-\dfrac{K_{23}K_{32}}{T_3} \end{bmatrix}, \tag{2a}$$

$$\tilde{d}=\begin{bmatrix} d_1-\dfrac{K_{13}d_3}{T_3} \\ d_2-\dfrac{K_{23}d_3}{T_3} \end{bmatrix}, \tag{2b}$$

where $T_i\equiv\tan\pi\nu_i+K_{ii}$. Since the zeroth-order positions of perturbers are determined by roots of $T_3=0$, it is clear that $\tilde{K}$ and $\tilde{d}$ are strongly energy dependent in the vicinity of perturbers. In other words, $\tilde{K}$ and $\tilde{d}$ carry all the information about the perturbers implicitly through their energy dependence.

It is now straightforward to obtain the continuum phase shift and the photoionization cross section analytically for this two-channel system by using standard MQDT methods [31]. That is, the "physical" phase shift Δ in the lone open channel can be obtained by solving a determinantal equation,

$$\det\begin{vmatrix} \tan(-\Delta)+\tilde{K}_{11} & \tilde{K}_{12} \\ \tilde{K}_{21} & \tan\pi\nu_2+\tilde{K}_{22} \end{vmatrix}=0, \tag{3a}$$

and the cross section is given by

$$\sigma=I_0\cos^2\Delta\left[\tilde{d}_1-\frac{\tilde{K}_{12}\tilde{d}_2}{\tan\pi\nu_2+\tilde{K}_{22}}\right]^2, \tag{3b}$$

where I_0 is proportional to the photon energy.

We stress, however, that our primary purpose in this paper is to study and develop a parametrization for detailed properties of a complex resonance, rather than to simply calculate the phase shift and cross section, which are already familiar procedures in conventional MQDT calculations. In particular we want to study how the intensity, line shape, and autoionization width of each individual resonance changes with energy when a perturber is embedded within the host Rydberg series. To accomplish this, we adopt the same formulation as Giusti-Suzor and Fano [20], who utilize an alternative set of parameters to treat a two-channel problem having an energy-independent K-matrix. These include two phase parameters $\{\tilde{\mu}_1,\tilde{\mu}_2\}$ and a pure channel-coupling matrix

$$\tilde{R}=\begin{bmatrix} 0 & \xi \\ \xi & 0 \end{bmatrix}$$

to parametrize the $\tilde{K}$ matrix. Notice that all of these parameters become energy dependent in the present problem owing to the elimination of the third channel discussed in Eq. (2). The MQDT elimination of channel 2 can now be achieved as in Eq. (3a) by solving the determinantal equation

$$\det\begin{vmatrix} \tan(-\Delta+\pi\tilde{\mu}_1) & \xi \\ \xi & \tan\pi(\nu_2+\tilde{\mu}_2) \end{vmatrix}=0 \tag{4}$$

giving the same phase shift Δ as Eq. (3a). Thus the relation between these parameters and the $\tilde{K}$ elements can be easily derived after several steps of algebraic manipulation:

$$\tilde{K}_{11}=\frac{\tan\pi\tilde{\mu}_1+\xi^2\tan\tilde{\mu}_2}{1-\xi^2\tan\pi\tilde{\mu}_1\tan\tilde{\mu}_2}, \tag{5a}$$

$$\tilde{K}_{22}=\frac{\tan\pi\tilde{\mu}_2+\xi^2\tan\tilde{\mu}_1}{1-\xi^2\tan\pi\tilde{\mu}_1\tan\tilde{\mu}_2}, \tag{5b}$$

$$\tilde{K}_{12}=\frac{1}{\cos\pi\tilde{\mu}_1\cos\pi\tilde{\mu}_2}\frac{\xi}{1-\xi^2\tan\pi\tilde{\mu}_1\tan\tilde{\mu}_2}. \tag{5c}$$

Inversion of Eqs. (5a)–(5c) yields the expression of each parameter:

$$\pi\tilde{\mu}_1=\tfrac{1}{2}\arctan\left[\frac{2(\tilde{K}_{11}+\tilde{K}_{22}D_K)}{1-D_K^2-(\tilde{K}_{11}^2-\tilde{K}_{22}^2)}\right]+\frac{n_1\pi}{2}, \tag{6a}$$

$$\pi\tilde{\mu}_2=\tfrac{1}{2}\arctan\left[\frac{2(\tilde{K}_{22}+\tilde{K}_{11}D_K)}{1-D_K^2-(\tilde{K}_{22}^2-\tilde{K}_{11}^2)}\right]+\frac{n_2\pi}{2}, \tag{6b}$$

$$\xi^2=\frac{[(\tilde{K}_{11}+\tilde{K}_{22})^2+(1-D_K)^2]^{1/2}-[(\tilde{K}_{11}-\tilde{K}_{22})^2+(1+D_K)^2]^{1/2}}{[(\tilde{K}_{11}+\tilde{K}_{22})^2+(1-D_K)^2]^{1/2}+[(\tilde{K}_{11}-\tilde{K}_{22})^2+(1+D_K)^2]^{1/2}}, \tag{6c}$$

with $n_{1,2}=0,1,2,\ldots$ and $D_K \equiv \det|\tilde{K}_{ij}|$. Some remarks are necessary to fully specify the energy-dependent parameters $\pi\tilde{\mu}_i$ and ξ, as there are an infinite number of possible branches for the $\pi\tilde{\mu}_i$. Since adding an integer multiple of π to $\pi\tilde{\mu}_i$ does not change the final cross section, only $n_{1,2}=0$ and 1 give physically different branches. Therefore, there are four possible branch combinations of $\pi\tilde{\mu}_i$. But not all of them give the correct spectrum. The signs of the numerator and denominator in the brace of Eq. (6a) can be used to determine the quadrants for $2\pi\tilde{\mu}_1$. Taking the sign of the numerator to coincide with the sign of $\sin 2\pi\tilde{\mu}_1$ and the sign of the denominator to coincide with the sign of $\cos 2\pi\tilde{\mu}_1$ uniquely determines the quadrant of $2\pi\tilde{\mu}_1$. The same procedure applies to determine the quadrant of $2\pi\mu_2$. As for the sign of ξ, it is uniquely determined as well through Eq. (5c) after determining $\tilde{\mu}_i$. Notice that ξ^2 in Eq. (6c) is always less than 1. When we calculate ξ^2 from Eqs. (5a)–(5c), we obtain another solution whose value is equal to the inverse of Eq. (6c), i.e., $\xi^2>1$. But it does not give any different physical solution to the problem. To see it more clearly, we know from Eqs. (5a)–(5c) that these equations are invariant under replacement of ξ^2 by $1/\xi^2$ provided one simultaneously replaces $\tilde{\mu}_i$ by $\tilde{\mu}_i+\frac{1}{2}$. Therefore, the $\xi^2>1$ case can be converted to the $\xi^2<1$ case, using care to change branches for the $\pi\tilde{\mu}_i$. The physical origin of this conversion has been already discussed in detail in Refs. [20] and [32], which point out that these replacements amount to interchanging the two eigenchannels of the $\tilde{K}$ matrix.

After obtaining $\tilde{\mu}_i$ and ξ, the photoionization cross section depends on the new set of parameters in the form

$$\sigma = I_0 \left[\cos(-\Delta+\pi\tilde{\mu}_1)\tilde{D}_1 - \sin(-\Delta+\pi\tilde{\mu}_1)\frac{\tilde{D}_2}{\xi} \right]^2 , \quad (7a)$$

where $\tilde{D}_1$ and $\tilde{D}_2$ are related to $\tilde{d}_1$ and $\tilde{d}_2$ by

$$\begin{aligned} \tilde{D}_1 &= \tilde{d}_1\cos\pi\tilde{\mu}_1 - \xi\tilde{d}_2\sin\pi\tilde{\mu}_2 , \\ \tilde{D}_2 &= -\xi\tilde{d}_1\sin\pi\tilde{\mu}_1 + \tilde{d}_2\cos\pi\tilde{\mu}_2 . \end{aligned} \quad (7b)$$

Equation (7a) can be rewritten in a form suggestive of a Fano profile:

$$\sigma = I_0\tilde{D}_1^2 \frac{\left[\cot(-\Delta+\pi\tilde{\mu}_1) - \frac{1}{\xi}\frac{\tilde{D}_2}{\tilde{D}_1}\right]^2}{1+\cot^2(-\Delta+\pi\tilde{\mu}_1)} . \quad (8)$$

The position of a resonance can be defined as the energy at which the phase shift varies most rapidly, or where the time delay is at a maximum. Since the parameter ε in a Beutler-Fano profile vanishes at the center of a resonance and can be written as $(E-E_R)/\frac{1}{2}\Gamma_R$ in its vicinity, we compare in Fig. 2 the two functions $[\cot(-\Delta+\pi\tilde{\mu}_1)]^{-1}$ and $d\Delta/d\nu_2$. (Since $d\Delta/d\nu_2$ relates to $d\Delta/dE$ in a simple way, i.e., $d\Delta/dE=\nu_2^{-3}d\Delta/d\nu_2$, $d\Delta/d\nu_2$ reaches its maximum at the same energy as $d\Delta/dE$.) From the graph it can be seen that the positions of the peaks of $d\Delta/d\nu_2$ correspond closely to the positions of poles of $[\cot(-\Delta+\pi\tilde{\mu}_1)]^{-1}$. This agreement implies that we should identify $\varepsilon \equiv \cot(-\Delta+\pi\tilde{\mu}_1)$. The quantity $-(1/\xi)(\tilde{D}_2/\tilde{D}_1)$ is similarly identified as the shape parameter, i.e., $q=-(1/\xi)(\tilde{D}_2/\tilde{D}_1)$. To justify these definitions, recall that the original idea of a Fano profile [25,26] requires the parameters σ_0, q, and Γ to be constant, or at least nearly independent of energy over the width of the resonance.

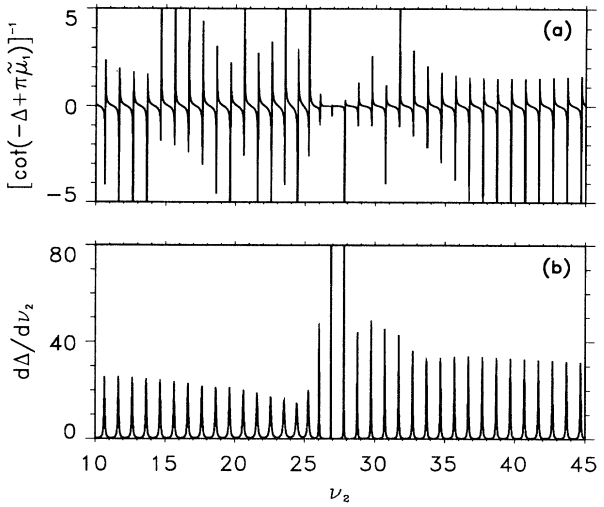

FIG. 2. (a) The function $[\cot(-\Delta+\tilde{\mu}_1)]^{-1}$ plotted vs the effective quantum number of the second channel, i.e., $\nu_2=[-2(E-E_2)]^{-1/2}$, showing many poles. (b) The derivative of the phase shift Δ with respect to ν_2, which has peaks lying close to the positions of the poles in (a).

We have calculated the photoionization spectrum and the q parameter for individual resonances, as defined above for a *broad interloper,* by using a symmetric K matrix with elements $K_{11}=-1.19$, $K_{12}=1.14$, $K_{13}=0.31$, $K_{22}=1.16$, $K_{23}=0.23$, and $K_{33}=-0.14$, and dipole matrix elements $d_1=0.95$, $d_2=-0.80$, and $d_3=0.40$. The channel structure for the model calculation consists of three equally spaced ionization thresholds, i.e., Landau thresholds ($n=0,1,2$) with $m=1$ and $\omega_c=0.0129$. These expressions for q and ε are appropriate only for a broad perturber, meaning specifically that the perturber is much broader in energy than the unperturbed energy-level separations of the host Rydberg series. The results for the cross section and q parameter are shown in Figs. 3(b) and 3(c). Dynamical information about the perturber position, width, and shape is also shown in Fig. 3(a) for clarity. From these graphs, a major qualitative conclusion is that while the q parameter is rather energy dependent across the width of the perturber, it is rather smooth across the width of most individual resonances. Some significant variations of q occur close to the center of the perturber near $\nu_2\approx 25$, where q oscillates from being a large negative number to being a large positive number (i.e., $\arctan q$ oscillates about the value $-\frac{1}{2}\pi$). However, the shapes of the actual resonances are hardly affected by this seemingly large oscillation in the values of q.

It should be stressed that it is not sufficient to arrange the cross section as in Eq. (8) so that it mimics the form

of the Beutler-Fano line shape. For instance, if the resulting q (or other) parameter is not roughly constant across an autoionizing resonance, the resulting line-shape parameters have little meaning. A definitive test of the above expressions derived for q, Γ, and E_R is to compare the exact photoionization cross section calculated using Eq. (8) to the resonant cross section using the Beutler-Fano line shape with constant parameters. Note that Γ_R has been approximated as the reciprocal of the time delay, $\Gamma_R = 2(d\Delta/dE)^{-1}|_{E=E_R}$. For narrow resonances (within a comparatively broad perturber), the Beutler-Fano line profile agrees quite well with the exact cross section, as can be seen from Fig. 4(a), where the solid line is the exact calculation and the dotted line is the Beutler-Fano profile calculated with constant parameters. For broad resonances, however, the agreement is somewhat poorer, as can be seen in Fig. 4(b). The discrepancy is largest at the wings of the resonance, which may stem from the close proximity of other resonances nearby, or to the neglect of the energy dependence of the q parameter. While it is clearly preferable to use the exact MQDT expression (8) directly for obtaining the quantitative spectrum, the general agreement of the Beutler-Fano parametrization suggests that the definitions of q, Γ, and E_R describe the overall shape of each individual resonance adequately.

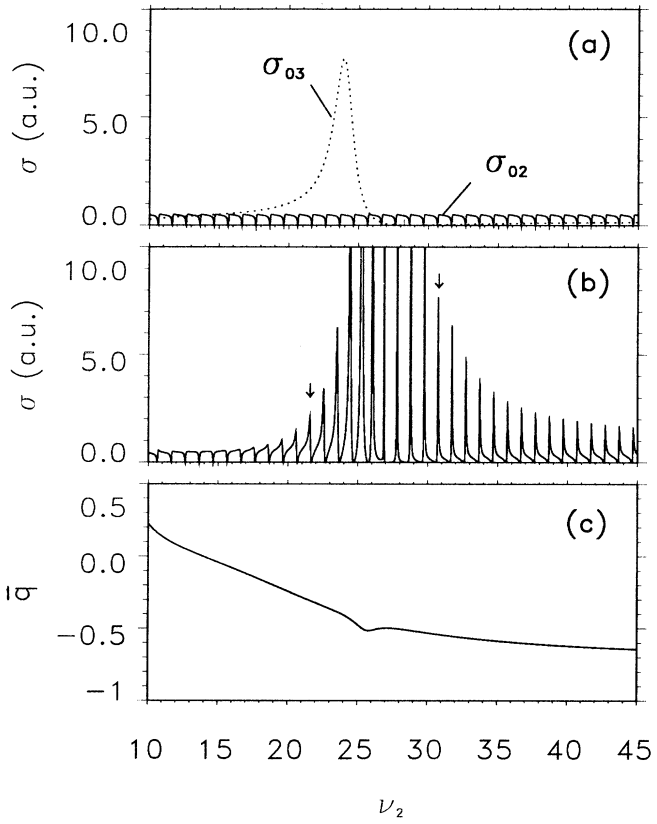

FIG. 3. (a) σ_{02} is the cross section calculated by assuming $K_{13}=K_{31}=K_{23}=K_{32}=0$. Under these assumptions, the states in the third channel are bound states of zero width. Thus the spectrum σ_{02} represents an unperturbed host Rydberg series. Similarly σ_{03} shows the perturber locations expected in the absence of interactions. This spectrum was calculated by setting $K_{12}=K_{21}=K_{23}=K_{32}=0$. (b) The cross section shown was calculated using the full K matrix, giving a perturbed autoionizing Rydberg series. The peaks with arrows are described by a Beutler-Fano profile in Fig. 4. (c) The Fano line shape q is shown as a plot of the quantity $\bar{q} \equiv \arctan q/\pi$, where q is defined below Eq. (8). Note that poles of q occur when $\bar{q}$ has the value $-\frac{1}{2}(\mathrm{mod}\,1)$. The q parameter has one zero and three poles in this calculation within the width (or nearly within the width) of each perturber.

A q parameter has also been identified for this three-channel MQDT problem by other authors. Wintgen and Friedrich [30] give an alternative identification by a different procedure. First, they arrange the cross section in the form of a Fano profile, after which a shape parameter is identified in their Eq. (24), which is a rapidly oscillating function of energy. To get physically correct q values, they subsequently evaluate q near the resonance energy, giving their Eq. (24'). The q obtained in this way is an approximation and valid for the case of narrow resonances, whereas our parametrization of q appears to be smoother and valid for both narrow and broad resonances. For the channel interaction parameters cited above, each perturber causes one zero of q, and three poles. We have also seen examples in our numerical "experiments" in which each perturber has one zero and one pole, which is the case predicted by Ref. [30]. These sign changes of q in our parametrization are clearly associated with changes in the asymmetry of individual resonances in Fig. 3(b). It can be seen from Fig. 3(c) that q reversals can occur either when q passes continuously through zero, or when q has a pole as a function of the energy. Almost always, the zeros of q cause a more noticeable

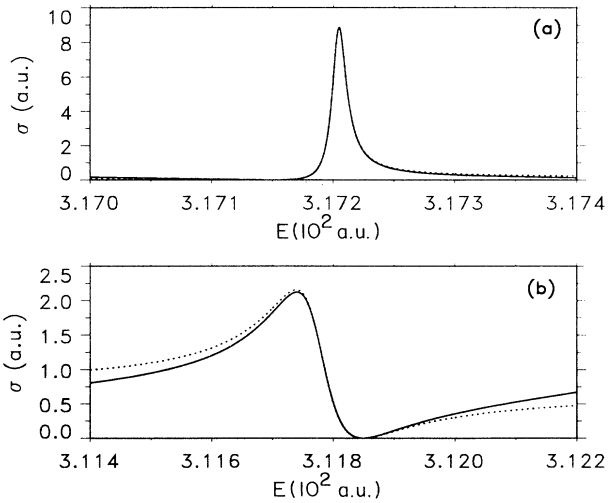

FIG. 4. Test of the Beutler-Fano profile parametrization developed in Eq. (8) for the resonances marked by arrows in Fig. 3(b). The solid curves represent exact MQDT calculations, while the dotted curves are the Beutler-Fano line shapes with constant parameters. (a) The resonance with $E=0.031\,72$, $\Gamma=1.43\times10^{-6}$, $q=7.71$, and $\sigma_0=0.15$. (b) The resonance with $E=0.031\,175$, $\Gamma=1.03\times10^{-5}$, $q=-1.43$, and $\sigma_0=0.71$.

change in the asymmetry of the actual resonances than do poles of q. As a rough rule of thumb, the poles of q tend to occur very close to the center of the perturber, whereas the zeros of q are farther out on the edges of the perturber.

A perturber also modifies the autoionization width of the individual members of the host Rydberg series. In the absence of perturbers, it is well known that the widths of successive resonances decay in proportion to ν_2^{-3}. For this reason, it is preferable to introduce a smoother "reduced decay width" equal to $\nu_2^3\Gamma$. Following the definition of Fano and Rau [32], we define the reduced width as $\Gamma^{(r)}=2/(\pi d\Delta/d\beta_2)$ (with $\beta_2=\pi\nu_2$). The explicit expression can be derived from Eq. (4),

$$\Gamma^{(r)}=\frac{2}{\pi}\xi^2\left[\xi^2\frac{d\tilde{\mu}_1}{d\nu_2}+\frac{1+\xi^4\varepsilon^2}{1+\varepsilon^2}\left[1+\frac{d\tilde{\mu}_2}{d\nu_2}\right]-\frac{\varepsilon}{1+\varepsilon^2}\frac{d\xi^2}{d\beta_2}\right]^{-1}. \tag{9a}$$

This is a rapidly oscillating function of the energy owing to the rapid oscillations of ε as defined above. A more suitable expression, which is smooth and which attains a physically correct value at the center of each individual resonance, is obtained by using the fact that $\varepsilon=0$ at the center of each resonance. The resulting reduced-width function is far smoother, and can be calculated from

$$\Gamma_s^{(r)}\equiv\frac{2}{\pi}\xi^2\left[1+\xi^2\frac{d\tilde{\mu}_1}{d\nu_2}+\frac{d\tilde{\mu}_2}{d\nu_2}\right]^{-1}. \tag{9b}$$

Figure 5 contrasts the rapid oscillations of $\Gamma^{(r)}$, which exhibit a dip at every resonance energy, with the smooth curve representing $\Gamma_s^{(r)}$. This smooth reduced-width curve passes through (or extremely close to) all the minima, displaying an asymmetric shape reminiscent of a Beutler-Fano line shape for the smooth width function itself.

The spectrum in Fig. 3(b) shows that the intensity of the perturber is redistributed among the host Rydberg states causing a great intensity enhancement for the high Rydberg states, where the perturber itself is no longer distinguishable from the host Rydberg series. Furthermore, the intensity enhancement and the influence on the widths and q parameters of the Rydberg series extend far beyond width of the perturber.

The asymmetric shape of $\Gamma_s^{(r)}$ gives us a hint that in one energy range the perturber decay to the continuum can interfere constructively with that of the host Rydberg series, thereby resulting in broader individual resonances. Elsewhere, however, the interference can be destructive, resulting in individual resonances that are narrower than the unperturbed host Rydberg series members. This feature is clearly visible in Fig. 3(b), where individual resonances are broadened on the lower-energy side of the complex resonance, but narrowed on the higher-energy side of this perturber. The destructive interference can cause another interesting phenomenon, namely *zero-width resonances*. Since the effect of destructive interference is to slow the autoionizing decay of a resonant state,

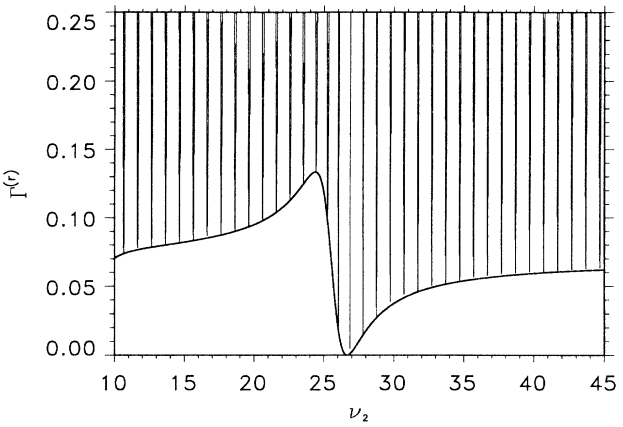

FIG. 5. The rapidly oscillating function is the reduced width function calculated from Eq. (9a). The solid curve is the smooth reduced width function, whose analytical form is given in Eq. (9b).

it can essentially become a true bound state in the continuum if the resonance width happens to vanish. This phenomenon has been discussed by Friedrich and Wintgen for atomic hydrogen in a magnetic field [2]. Figure 5 also shows that the function $\Gamma_s^{(r)}$ has a zero. When the field strength is varied, the energy of a resonant state can be made to coincide with this point, where it becomes such a "bound state in the continuum." This zero-width resonance usually lies very close to the center of the perturber, and simultaneously the q value approaches infinity, as expected since the oscillator strength distribution for a transition to a bound level has the form $df/dE=f_n\delta(E-E_n)$.

The preceding derivation of the cross section in the form (8), by first eliminating channel 3 followed by the elimination of channel 2, is exact. However, the identification of the Beutler-Fano line-shape parameters Γ, q, and σ_0 based on this form of the cross section becomes inappropriate whenever the perturber width becomes small enough so that it is comparable to, or less than, the separation between levels of the host Rydberg series. In this limit of a narrow perturber, the perturbing resonance can be distinguished from the Rydberg levels in the second channel, and its Γ,q values can be calculated separately. The approach developed in Eq. (2) and in Eqs. (7) and (8) remains valid for a narrow perturber provided channel 2 is eliminated first instead of channel 3. Thus if labels 2 and 3 are everywhere interchanged, Eq. (8) still gives a Beutler-Fano parametrization in this limit.

III. THE EFFECT OF THRESHOLDS VARYING WITH A MAGNETIC FIELD

Now we consider the evolution of the properties of a complex resonance as functions of a changing magnetic

field. The Landau threshold energies are proportional to the magnetic field, with slopes $dE_i/d\omega_c = [n+(|m|+m+1)/2]$. Here the MQDT channel index $i=1,2,\ldots$ corresponds to the Landau quanta $n=0,1,\ldots$. The Rydberg structures associated with different channels are differentiated by observing their field dependence. For a high Rydberg resonance state that is unperturbed, the energy can be expressed in a simple form $E_{i,n_z}=E_i-1/(2n_z^{*2})$, where $n_z^*=n_z-\mu_z$ is the effective quantum number in channel i. The quantum defect μ_z is a generally smooth function of both magnetic field and energy. If the state is high enough, μ_z can be regarded as energy independent. In this limit the resonance energy has a slope with changing magnetic field given by

$$\frac{dE_{i,n_z}}{d\omega_c}=\left[n+\frac{|m|+m+1}{2}\right]-\frac{d\mu_z}{d\omega_c}\frac{1}{(n_z-\mu_z)^3}\,. \tag{10}$$

This expression shows that the slope of sufficiently high Rydberg levels coincides with the slope of the corresponding ionization threshold, since the last term in Eq. (10) becomes arbitrarily small as $n_z\to\infty$. Consequently states in higher channels have larger slopes than states in lower channels, as shown in the experimental study of Li diamagnetism by Iu *et al.* [1] in Fig. 6. For relatively low states in each channel, since they interact strongly with states in other channels and in some cases appear as broad perturbers, the slopes are difficult to evaluate. Figure 7 shows our calculated spectrum as a function of both the magnetic field and the energy. This model calculation is performed by assuming a three-channel K matrix to be independent of both B and E, so that the only field dependence is contained in the ionization threshold energies. The three channels included are the Landau channels with $n=0$, 1, and 4.

Several interesting features can be seen that resemble experimental features from Ref. [1]. First of all, resonances with different slopes versus B are evident in the spectrum, as well as avoided crossings at the intersections between two Rydberg states. This feature is very obvious in the experiment, where widely spaced intense lines having large slopes are seen to cross families of weaker, narrowly spaced levels with small slopes. The reason the

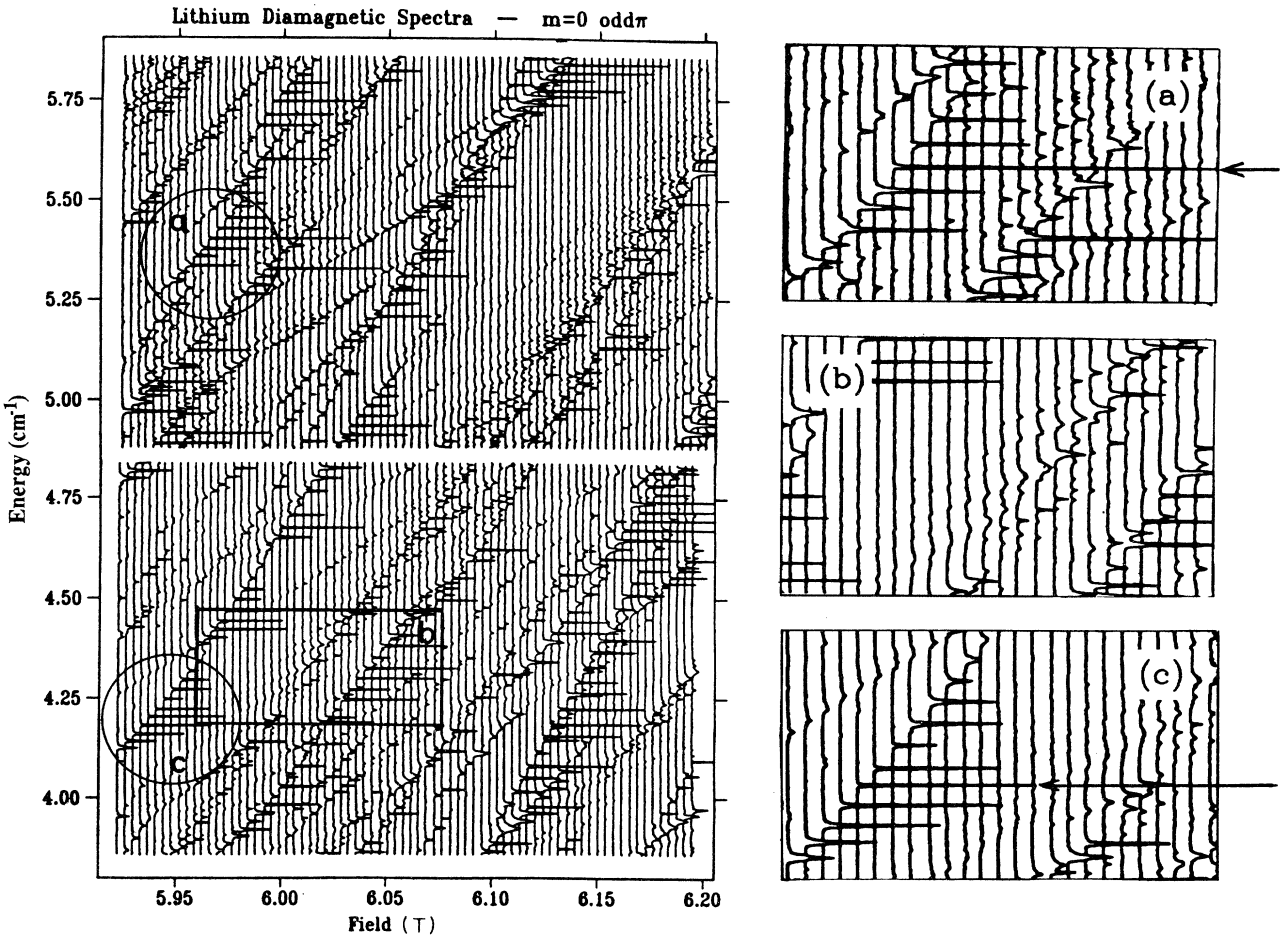

FIG. 6. Experimental spectrum of lithium in a magnetic field, observed by Iu *et al.* in Ref. [1]. (a) The observation of a q reversal associated with a pole of q. (b) An example of state intensities diminishing, in fact dissipating altogether as the field is decreased. (c) Possible observation of a zero-width resonance.

states with larger slopes have a greater energy spacing than lower-slope states stems from the fact that, in a given energy range, the states having larger slopes are lower-n_z Rydberg states in higher channels, whose spacing is roughly $(n_z^*)^{-3}$. Some bending of these levels away from straight lines is a manifestation of the interaction between different Rydberg channels.

The variation of the q parameter with E and B is another important factor that influences the appearance of the spectrum in Fig. 7. As discussed in the preceding section, poles of q tend to occur very close to the center of the perturber. A q reversal associated with a pole of q can be seen in the experimental spectrum [1] shown in circle (a) in Fig. 6, where the resonance intensities are rather high because of being close to the center of the perturber. At lower energy and field, the resonance has a negative q value. As the field increases, the q value changes quickly to positive values. When a q reversal happens around $q=0$, an interesting intensity variation becomes noticeable. In Fig. 7 we plot two dashed lines where $q=0$ is expected. These lines can be obtained numerically from the definition of $q=-(1/\xi)(\tilde{D}_2/\tilde{D}_1)$, that is, $\tilde{D}_2=0$ (since ξ, $\tilde{D}_1$, and $\tilde{D}_2$ are finite in our calculation). They form nearly straight lines with slopes larger than that of second threshold. As is well known, and can

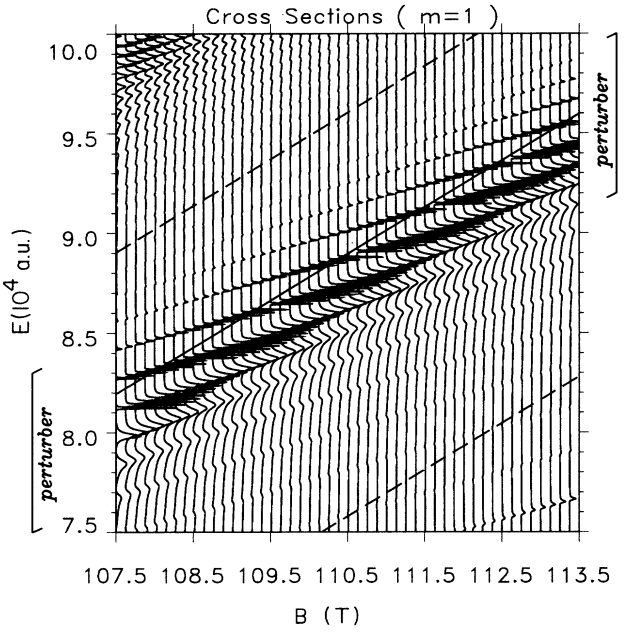

FIG. 7. Evolution of a complex resonance with the magnetic field. The MQDT spectrum is calculated by using a constant three-channel K matrix with elements $K_{11}=-1.3$, $K_{12}=1.1$, $K_{13}=0.94$, $K_{22}=1.1$, $K_{23}=0.38$, and $K_{33}=-0.26$, and with dipole matrix elements $d_1=1.20$, $d_2=-0.85$, and $d_2=0.50$. The channel structure consists of three Landau channels $E_i=(\omega_c/2)(2n+|m|+m+1)$, with $i=1,2,3$ corresponding to $n=0,1,4$, respectively, and with $m=1$. The spectrum has been convoluted with a Gaussian of full width at half maximum 2.5×10^{-7} (a.u.). The solid line in the plot is the zero-width line as discussed in the text, and the dashed lines are $q=0$ lines.

be seen from the Fano line-shape formula, the cross section reaches its minimum at the resonance energy, if $q=0$. If we pick one single resonance in the upper half plane of (E,B) in Fig. 7, and follow its evolution as B decreases, the resonance intensity is seen to decrease as it approaches the $q=0$ curve, minimizing near this line. After passing the line, the resonance intensity increases again while the line-shape asymmetry q changes sign. Therefore, the intensities of resonances are generally very small close to the $q=0$ curves. In the experimental spectrum in area (b), we see some examples where resonance intensities diminish out on the edge of the complex resonance, with small q values. However, no example of such a q reversal around $q=0$ could be found in this experiment, since the strong peaks all have large q values. Because a q reversal associated with $q=0$ usually happens on the edge of a complex resonance and it is rather gradual as well, the reversal process takes a wide range of E or B to complete. Therefore, it extends considerably beyond the width of the perturber. At a field strength around 6 T, a larger number of interacting channels (approximately 30) are involved. The experimental spectrum is accordingly far more complicated than that of this simple model. Despite our difficulty in observing $q=0$ states in Ref. [1], our analysis using this simple model predicts that the frequent "disappearance" of resonances, evident in the observed spectra [1], could be caused by the $(q=0)$-type q reversals.

The asymmetric constructive and destructive interferences also cause another characteristic feature in Fig. 7. That is, just above and to the left of the perturber marked on Fig. 7, the resonance widths are comparatively narrow, while at an equal distance below and to the right of the perturber, the individual resonance widths are broader. The experimental spectrum [1] displays similar asymmetries, which are barely visible in Fig. 6(c). That is, the fourth resonance below and to the right of the marked resonance in Fig. 6(c) is visibly broader than the fourth resonance above to the left of the marked one. Such an asymmetric shape of the width function has already been seen in Fig. 5. There the dip in the higher-energy regime indicates destructive interference, while the peak in the lower-energy regime indicates constructive interference.

As we have noticed from experiments [18], there always exist very narrow resonances, even well above the first ionization threshold. This can be explained as the effect of destructive interference between different autoionization pathways. Our model calculation shows that for any fixed magnetic-field strength, there are zero-width points at certain energies, although at most values of B no resonance lies at those special energies. If there is no interaction between the closed channel and the open channel, as implied by zero width, the autoionization states in the closed channel are essentially true bound states. Based on this fact, we can give an analytical expression of zero-width points in the (E,B) plane by setting $\tilde{K}_{1,2}=0$. The explicit expression is then

$$E=E_3-\frac{1}{2(n_z-\delta)^2}\ , \tag{11a}$$

where δ is defined as

$$\delta=\frac{1}{\pi}\arctan\left[K_{3,3}-\frac{K_{1,3}K_{3,2}}{K_{1,2}}\right]. \tag{11b}$$

Equation (11a) describes a straight line for E versus B, whose slope coincides with the slope of the third threshold energy. The solid line in Fig. 7 shows the zero-width resonance positions, demonstrating how the resonances close to this line are narrower than the resonances further away from it. Note that in Fig. 7, the resonances lying near this line are not fully resolved, which is an artifact of the finite mesh used in the theoretical calculation. In fact the integrated "strength" across such resonances remains finite and smooth even as their widths go through zero.

In circle (c) of Fig. 6, an experimental example is shown of a resonance width decreasing as E and B increase. Up to a certain point in the lower half of Fig. 6(c), the resonance is seen to get increasingly narrow, high, and symmetric. The marked resonance has maximum intensity and minimum width. Beyond this marked resonance, the width again increases, while at the same time its shape becomes somewhat more asymmetric and the intensity diminishes again. This appears to be an experimental example of a zero-width resonance. Moreover, the resonance intensity distribution near this possible zero-width point is very similar to that in the model spectrum shown in Fig. 7.

The evolution of a complex resonance for this three-channel system is very tractable and clear. It is characterized by two dynamical quantities, namely the width function and the shape parameter, which control the appearance of the spectrum. This analysis serves as a prototype for understanding more complicated systems. Figure 8 tests this description of Rydberg state diamagnetism by performing a similar model calculation near $B=6$ T, with twenty interacting channels converging to the $m=0$ Landau thresholds $E_i=\omega_c(i-\frac{1}{2})$, $i=1,2,\ldots,20$. The 20×20 K matrix and the twenty dipole matrix elements were chosen in essentially a random fashion, and then kept independent of E and B. The main point of this calculation is that it produces a spectrum having a complexity comparable to the experimental spectrum of Ref. [1], shown in Fig. 6. There are also numerous similar features in Figs. 6 and 8, including resonances with different "slopes" of E versus B, avoided crossings between individual resonances, and high Rydberg state resonances that fade in and out when traced versus E and B. This example is highly suggestive that the picture of a multichannel Rydberg spectrum will in fact be adequate to describe atomic diamagnetism near the zero-field ionization threshold.

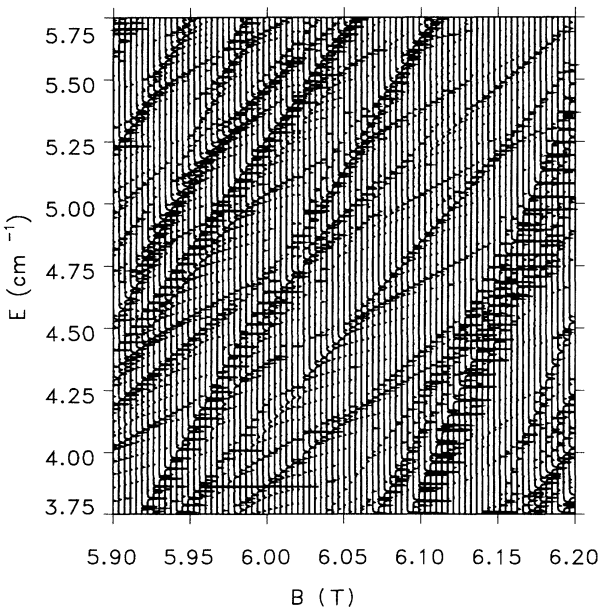

FIG. 8. Model MQDT spectrum is obtained for a system of 20 interacting Rydberg series converging to equally spaced Landau channels with $m=0$. The K matrix is chosen to be independent of energy and magnetic field. The spectrum plotted is a convolution with a Gaussian whose width is 0.001 cm^{-1}, to simulate the finite experimental resolution of Ref. [1].

IV. CONCLUSIONS

The problem of electron motion in the combination of a spherical Coulomb potential and a cylindrical diamagnetic potential has been compared [33] to the problem of two-electron motion near the threshold for double escape. Similarities do exist between them, primarily in the fact that each involves a nonseparable Schrödinger equation in just a few degrees of freedom, and also in the fact that resonances are established along a potential ridge in each problem. The diamagnetism of Rydberg atoms, however, is much simpler in principle, because at any given energy there is a finite number of interacting Landau channels. (In this sense it is analogous to the two-electron problem at energies just *below* the double-escape threshold.) The asymptotic channel structure is therefore quite clear [9], and in particular the asymptotic wave function at $|z|\rightarrow\infty$ is a straightforward Landau channel expansion, each of whose terms is separable in cylindrical coordinates. On the other hand, the two-electron continuum wave function in the field of a central charge appears to remain nonseparable all the way out to infinity near threshold.

Viewed from this perspective, it is clear that in any given energy range, the motion of a bound or continuum Rydberg electron in a magnetic field must be describable within the framework of the standard multichannel quantum-defect theory. This description of N interacting Landau channels is based on an $N\times N$ "smooth" reaction matrix K_{ij}, with an additional N dipole matrix element d_j needed to calculate the photoabsorption spectrum. Difficulties of a practical nature have made the calculation of this information $\{K_{ij},d_j\}$ prohibitively time consuming for two reasons: (i) The large number of interacting channels $N\approx20-30$ in the near-threshold energy range for a 6-T magnetic field; (ii) the large volume over which the wave function is nonseparable for a 6-T field, roughly a cylinder of radius $\gtrsim10^3$ a.u. and of comparable length. The determination of an accurate $\{K_{ij},d_j\}$ re-

quires an accurate numerical solution of the Schrödinger equation throughout this volume.

Variational [22] or close-coupling-type [34] methods have successfully calculated $\{K_{ij},d_j\}$ for ultrastrong fields $B \gtrsim 10^3$ T, but to lower B another two orders of magnitude looks very difficult with existing methods. A line of attack that is particularly promising is the development of a spherical-to-cylindrical coordinate frame transformation approach by O'Mahony [24]. This has already produced good results near 100 T and appears capable of treating substantially lower fields without any great modification in principle. A related treatment developed by Watanabe [35] has also found encouraging preliminary results at 6 T.

While the development of computational techniques capable of determining the MQDT parameters $\{K_{ij},d_j\}$ is an important final step, the present study has shown that many of the characteristic types of interference phenomena can be classified without knowing these parameters. The evolution of perturbers and "complex resonances" as functions of energy and magnetic field has considerable complexity, even when $\{K_{ij},d_j\}$ are independent of E and B as in the model calculations of Sec. III. We have seen how many complex features of the type observed in lithium by Iu *et al.* [1] are generated by just three interacting Rydberg channels attached to Landau thresholds. The last example of Sec. III shows how a 20-channel calculation should, in principle, be able to describe the complete spectrum of Ref. [1], although the complete demonstration using an *ab initio* K matrix remains a task for subsequent studies. The recent success of Delande, Bommier, and Gay [11] in reproducing the experiments of Refs. [1] and [12] is an impressive demonstration of computational power. A partial interpretation of the many interfering resonances is pointed out by Ref. [11], but it is difficult to pinpoint the key physical processes, as the spectrum emerges from diagonalization of a $90\,000 \times 90\,000$ matrix. Reduction of the information contained in this huge matrix to the more manageable number ($\lesssim 30$) of interacting Landau channels in a quantum-defect picture should ultimately simplify the job of interpretation, which remains to be completed.

ACKNOWLEDGMENTS

This work was supported in part by the U.S. Department of Energy. We thank D. Kleppner for discussions, and for providing unpublished experimental spectra. Comments on the manuscript by F. Robicheaux are also appreciated.

[1] Chun-ho Iu, George R. Welch, Michael M. Kash, Long Hsu, and Daniel Kleppner, Phys. Rev. Lett. **63**, 1133 (1989); and (private communications).
[2] H. Friedrich and D. Wintgen, Phys. Rev. A **32**, 3231 (1985); **31**, 3964 (1985).
[3] J. P. Connerade, and A. M. Lane, J. Phys. B **18**, L605 (1985); **20**, 1757 (1987); J. P. Connerade, A. M. Lane, and M. A. Baig, J. Phys. B **18**, 3507 (1985); A. M. Lane, *ibid.* **17**, 2213 (1984).
[4] J. Neukammer, H. Rinneberg, G. Jönsson, W. E. Cooke, H. Hieronymus, A. König, K. Vietzke, and H. Spinger-Bolk, Phys. Rev. Lett. **55**, 1979 (1985).
[5] Chris H. Greene and Longhuan Kim, Phys. Rev. A **36**, 2706 (1987).
[6] Ning Yi Du and Chris H. Greene, J. Chem. Phys. **85**, 5430 (1986).
[7] Chris H. Greene and Ch. Jungen, Adv. At. Mol. Phys. **21**, 51 (1985).
[8] Ch. Jungen and D. Dill, J. Chem. Phys. **73**, 3338 (1980).
[9] Qiaoling Wang and Chris H. Greene, Phys. Rev. A **40**, 742 (1989).
[10] C. Liu and A. F. Starace, Phys. Rev. A **35**, 467 (1987).
[11] D. Delande, A. Bommier, and J. C. Gay, Phys. Rev. Lett. **66**, 141 (1991).
[12] Chun-lo Iu, George T. Welch, Michael M. Kash, Daniel Kleppner, D. Delande, and J. C. Gay, Phys. Rev. Lett. **66**, 145 (1991).
[13] A. Holle, G. Wiebush, J. Main, K. H. Welge, G. Zeller, G. Wunner, T. Ertl, and H. Ruder, Z. Phys. D **5**, 279 (1987).
[14] J. Main, G. Wiebush, A. Holle, and K. H. Welge, Phys. Rev. Lett. **57**, 2789 (1986).
[15] D. Wintgen and H. Friedrich, Phys. Rev. A **36**, 131 (1987).
[16] M. A. Al-Laithy, P. F. O'Mahony, and K. T. Taylor, J. Phys. B **19**, L773 (1986).
[17] M. L. Du and J. B. Delos, Phys. Rev. Lett. **58**, 1731 (1987); Phys. Rev. A **38**, 1896 (1988); **38**, 1913 (1988).
[18] G. R. Welch, Michael M. Kash, Chun-ho Iu, Long Hsu, and Daniel Kleppner, Phys. Rev. Lett. **62**, 1975 (1989).
[19] L. A. Collins, B. I. Schneider, C. J. Noble, C. W. McCurdy, and S. Yabushita, Phys. Rev. Lett. **57**, 980 (1986); J. A. Stephens and V. McKoy, *ibid.* **62**, 889 (1989); B. Yoo, Ph.D. thesis, Department of Physics, Louisiana State University (1990).
[20] A. Giusti-Suzor and U. Fano, J. Phys. B **17**, 215 (1984).
[21] A. Giusti-Suzor and H. Lefebvre-Brion, Phys. Rev. A **30**, 3057 (1984).
[22] Qiaoling Wang and Chris H. Greene (unpublished).
[23] Chris H. Greene, Phys. Rev. A **28**, 2209 (1983); *Fundamental Processes in Atomic Dynamics,* in Vol. 181 of *NATO Advanced Study Institute Series B: Physics,* edited by J. S. Briggs, H. Kleinpoppen, and H. O. Lutz (Plenum, New York, 1988), p. 105.
[24] P. F. O'Mahony, Comments At. Mol. Phys. **25**, 309 (1991).
[25] U. Fano, Phys. Rev. **124**, 1866 (1961).
[26] U. Fano and J. W. Cooper, Phys. Rev. **137**, A1364 (1964).
[27] Frederick H. Mies, Phys. Rev. **175**, 164 (1968).
[28] J. P. Connerade, *Fundamental Processes in Atomic Dynamics,* Vol. 181 of *NATO Advanced Study Institute Series B: Physics,* edited by J. S. Briggs, H. Kleinpoppen, and H. O. Lutz (Plenum, New York, 1988), p. 565.
[29] W. E. Cooke and C. L. Cromer, Phys. Rev. A **32**, 2725 (1985).
[30] D. Wintgen and H. Friedrich, Phys. Rev. A **35**, 1628 (1987).
[31] M. J. Seaton, Rep. Prog. Phys. **46**, 167 (1983).
[32] U. Fano and A. R. P. Rau, *Atomic Collisions and Spectra* (Academic, Orlando, 1986).
[33] U. Fano, Phys. Rev. A **22**, 2660 (1980).
[34] A. Alijah, J. Hinze, and J. T. Broad, J. Phys. B **23**, 45 (1990).
[35] S. Watanabe (unpublished).